Eur. Phys. J. A **17**, 323–327 (2003)
DOI 10.1140/epja/i2002-10169-6

THE EUROPEAN PHYSICAL JOURNAL A

Neutron electric form factor up to $Q^2 = 1.47$ $(\mathrm{GeV/c})^2$

R. Madey[1,2,a], A.Yu. Semenov[1], S. Taylor[3], A. Aghalaryan[4], E. Crouse[5], G. MacLachlan[6], B. Plaster[3], S. Tajima[7], W. Tireman[1], Chenyu Yan[1], A. Ahmidouch[8], B.D. Anderson[1], H. Arenhövel[9], R. Asaturyan[4], O. Baker[10], A.R. Baldwin[1], H. Breuer[11], R. Carlini[2], E. Christy[10], S. Churchwell[7], L. Cole[10], S. Danagoulian[2,8], D. Day[12], M. Elaasar[13], R. Ent[2], M. Farkhondeh[3], H. Fenker[2], J.M. Finn[5], L. Gan[10], K. Garrow[2], P. Gueye[10], C. Howell[7], B. Hu[10], M.K. Jones[2], J.J. Kelly[11], C. Keppel[10], M. Khandaker[14], W.-Y. Kim[15], S. Kowalski[3], A. Lung[2], D. Mack[2], D.M. Manley[1], P. Markowitz[16], J. Mitchell[2], H. Mkrtchyan[4], A. Opper[6], C. Perdrisat[5], V. Punjabi[14], B. Raue[16], T. Reichelt[17], J. Reinhold[16], J. Roche[5], Y. Sato[10], I.A. Semenova[1], W. Seo[15], N. Simicevic[18], G. Smith[2], S. Stepanyan[4], V. Tadevosyan[4], L. Tang[10], P. Ulmer[19], W. Vulcan[2], J.W. Watson[1], S. Wells[18], F. Wesselmann[12], S. Wood[2], Chen Yan[2], S. Yang[15], L. Yuan[10], W.-M. Zhang[1], H. Zhu[12], and X. Zhu[10]

[1] Kent State University, Kent, OH 44242, USA
[2] Thomas Jefferson National Accelerator Facility, Newport News, VA 23606, USA
[3] Massachusetts Institute of Technology, Cambridge, MA 02139, USA
[4] Yerevan Physics Institute, Yerevan 375036, Armenia
[5] The College of William and Mary, Williamsburg, VA 23187, USA
[6] Ohio University, Athens, OH 45701, USA
[7] Duke University, Durham, NC 27708, USA
[8] North Carolina A&T State University, Greensboro, NC 27411, USA
[9] Johannes Gutenberg-Universität Mainz, D-55099 Mainz, Germany
[10] Hampton University, Hampton, VA 23668, USA
[11] University of Maryland, College Park, MD 20742, USA
[12] University of Virginia, Charlottesville, VA 22904, USA
[13] Southern University at New Orleans, New Orleans, LA 70126, USA
[14] Norfolk State University, Norfolk, VA 23504, USA
[15] Kyungpook National University, Taegu 702-701, Korea
[16] Florida International University, Miami, FL 33199, USA
[17] Rheinische Friedrich-Wilhelms-Universität Bonn, D-53115 Bonn, Germany
[18] Louisiana Tech University, Ruston, LA 71272, USA
[19] Old Dominion University, Norfolk, VA 23508, USA

Received: 1 November 2002 /
Published online: 15 July 2003 –

Abstract. The ratio of the electric to the magnetic form factor of the neutron, $g \equiv G_{En}/G_{Mn}$, was measured via recoil polarimetry (R.G. Arnold, C.E. Carlson, F. Gross, Phys. Rev. C **23**, 363 (1981)) from the quasielastic $^2\mathrm{H}(\vec{e}, e'\vec{n})^1\mathrm{H}$ reaction at three values of Q^2 (viz, 0.45, 1.15, and 1.47 $(\mathrm{GeV}/c)^2$) in Hall C of the Thomas Jefferson National Accelerator Facility. The data reveal that G_{En} continues to follow the Galster parameterization up to $Q^2 = 1.15$ $(\mathrm{GeV}/c)^2$ and rises above the Galster parameterization at $Q^2 = 1.47$ $(\mathrm{GeV}/c)^2$.

PACS. 14.20.Dh Properties of specific particles: Protons and neutrons – 24.70.+s Nuclear reactions: Polarization phenomena in reactions – 13.40.Gp Specific reactions and phenomenology: Electromagnetic form factors

1 Introduction

The electric form factor of the neutron, G_{En}, is a fundamental quantity needed for understanding both nucleon and nuclear structure. The Jefferson Laboratory E93-038 Collaboration [1] conducted quasielastic scattering measurements on a liquid-deuterium target at three values of Q^2 (viz, 0.45, 1.15, and 1.47 $(\mathrm{GeV}/c)^2$), the squared four-momentum transfer.

[a] e-mail: madey@jlab.org

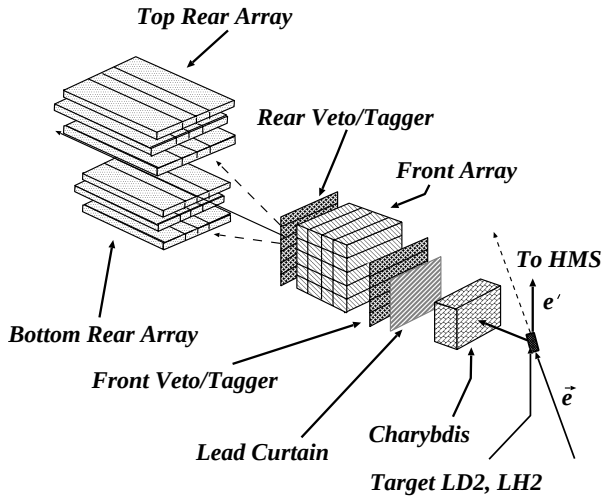

Fig. 1. Isometric view of the experimental arrangement.

2 Description of the experiment

An isometric view of the experimental arrangement is shown in fig. 1. A beam of longitudinally polarized electrons scattered quasielastically from a neutron in a 15 cm liquid-deuterium target. The polarization vector of the recoil neutron consists of two components in the scattering plane: a longitudinal component, $P_{L'}$, and a transverse (sideways) component, $P_{S'}$, parallel and perpendicular, respectively, to the momentum vector of the neutron. The scattered electron was detected in the High-Momentum Spectrometer (HMS) in coincidence with the recoil neutron. A neutron polarimeter (NPOL) [2] measured the up-down scattering asymmetry from a transverse component of the neutron's polarization vector. The dipole magnet (Charybdis) ahead of NPOL precessed the neutron's polarization vector through an angle χ. The polarimeter consisted of 20 detectors in the front array and 12 detectors in each of the two (upper and lower) rear arrays for a total of 44 plastic scintillation detectors. A double layer of "veto/tagger" detectors directly ahead of and behind the front array identified charged particles. To permit high luminosity, the detectors in each rear array were shielded from the direct path of neutrons from the target, and the 100 cm × 10 cm × 10 cm dimensions of each scintillator in the front array were small enough to accept high singles rates with luminosities up to $\sim 3 \times 10^{38}$ cm^{-2} s^{-1}. Each layer of the rear array consisted of two central scintillators, each 25.4 cm × 10.2 cm × 101.6 cm, with a 50.8 cm × 10.2 cm × 101.6 cm scintillator on each side. A 10 cm Pb curtain attenuated the flux of electromagnetic radiation and cut off the low-energy part of the spectra of charged particles incident on the polarimeter; the singles rate in a front veto detector was nearly five times higher with a 5 cm Pb curtain. The flight path from the target to the center of the front array was 7.0 m.

The basic equation [3] for the ratio of the electric to the magnetic form factor of the neutron, $g \equiv G_{En}/G_{Mn}$, is

$$g = -K_R \, (P_{S'}/P_{L'}) \tag{1}$$

Table 1. Kinematics.

Q^2 (GeV/c)^2	E_e (GeV)	θ_e (deg)	P_e (MeV/c)	P_n (MeV/c)	T_n (MeV)
0.45	0.884	52.65	643	711	239
1.14	2.326	30.93	1718	1227	606
1.17	2.415	30.15	1789	1249	624
1.47	3.395	23.55	2606	1448	786

with

$$K_R = \sqrt{\tau \left[1 + (1+\tau)\tan^2(\theta_e/2)\right]} \; ; \quad \tau \equiv Q^2/4\,M^2 \; .$$

Here the kinematic function K_R depends on the electron scattering angle θ_e and the squared four-momentum transfer Q^2. We utilized the neutron spin-precession dipole magnet, Charybdis, in two different ways to measure $P_{S'}$ and $P_{L'}$. In the first case, with the magnet off, we measured the scattering asymmetry $\xi_{S'}$ from the sideways component of polarization $P_{S'}$. Then with the magnet current selected to precess the neutron polarization vector through 90°, we measured the scattering asymmetry $\xi_{L'}$ from the longitudinal component of polarization $P_{L'}$. The ratio of polarizations, $P_{S'}/P_{L'}$, is equal to the ratio of associated scattering asymmetries, $\xi_{S'}/\xi_{L'}$, provided the beam polarization does not change during the sequential measurements of $P_{S'}$ and $P_{L'}$,

$$g = -K_R \, (\xi_{S'}/\xi_{L'}) \; . \tag{2}$$

In the second case, we select the Charybdis current to precess the neutron spin through $\pm\chi$ degrees. The top-bottom asymmetry measured in the neutron polarimeter is proportional to the projection of the neutron polarization vector on the axis that is perpendicular to the neutron momentum direction; in this case,

$$g = -K_R \left(\frac{1+\eta}{1-\eta}\right) \tan\chi \; ; \qquad \eta \equiv \xi_-/\xi_+ \; . \tag{3}$$

In addition to eqs. (2) and (3), g can be written in terms of the angle δ between the neutron polarization vector and the z-axis,

$$g = -K_R \, \tan\delta \; . \tag{4}$$

The kinematic conditions for each of the measured Q^2 points are listed in table 1. The central neutron kinetic energies range from 239 to 786 MeV. We measured each Q^2 point with a neutron spin precession angle of ±40°; also we measured the points at $Q^2 = 1.15$ and 1.47 (GeV/c)^2 with neutron spin precession angles of 0°, ±90°. For a neutron scattering angle of 46.0°, central Q^2 values of 0.45 and 1.47 (GeV/c)^2 were associated with beam energies of 0.884 and 3.395 GeV, respectively. The measurement we report at $Q^2 = 1.15$ (GeV/c)^2 is a weighted average of the "±40°" data collected at $Q^2 = 1.17$ (GeV/c)^2 at a beam energy of 2.42 GeV and the "0°, ±90°" data collected at $Q^2 = 1.14$ (GeV/c)^2 at a beam energy of 2.33 GeV.

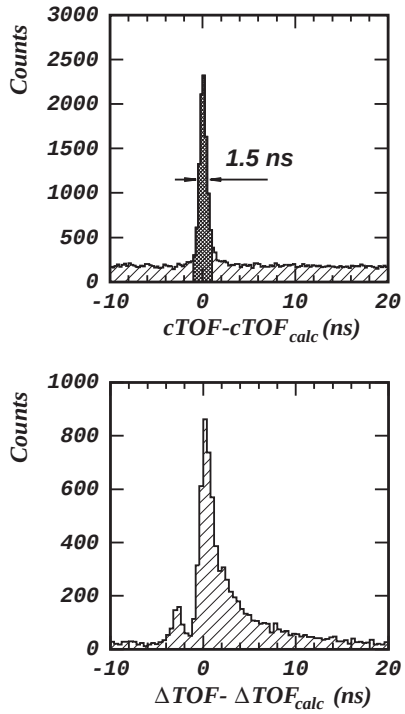

Fig. 2. Typical time-of-flight spectra.

3 Extraction of scattering asymmetries

Typical time-of-flight spectra are shown in fig. 2. The upper panel is an HMS-NPOL coincidence time-of-flight (cTOF) spectrum for $p(n,n)p$ elastic scattering events generated by neutrons incident on the polarimeter. Plotted on the abscissa is the difference between the measured flight time from the target to the front array and that calculated for a quasielastic neutron. The lower panel is the time-of-flight spectrum, termed ΔTOF, for a neutron event in the front array and a neutron in the rear array. Plotted on the abscissa is the difference between the measured flight time from the front array to the rear array minus that calculated for a neutron scattered elastically from a proton; this difference is scaled to a nominal mean flight path of 2.50 m. In this ΔTOF spectrum, the secondary peak centered at ~ -2.5 ns is the result of π^0 production in one of the scintillators in the front array. After decomposing the ΔTOF spectrum into four distinct ΔTOF spectra that depend on the helicity state of the beam and whether the scattering is to the upper or lower rear array, we extracted the yields in the main ΔTOF peak for each of these four spectra and calculated the cross ratio r:

$$r \;=\; \left(\frac{N_U^+\; N_D^-}{N_U^-\; N_D^+}\right)^{1/2} \;. \qquad (5)$$

Here N_U^+ (N_D^-) is the yield in the ΔTOF peak for particles scattered up (down) when the beam helicity was positive (negative). The physical scattering asymmetry is then given by

$$\xi \;=\; (r-1)/(r+1)\;. \qquad (6)$$

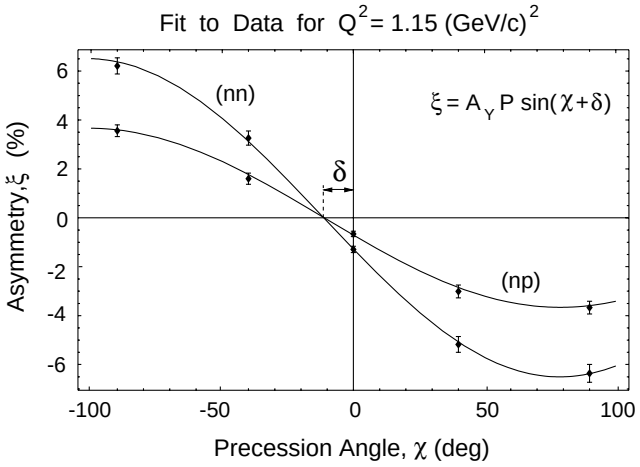

Fig. 3. Scattering asymmetries *vs.* scattering angle.

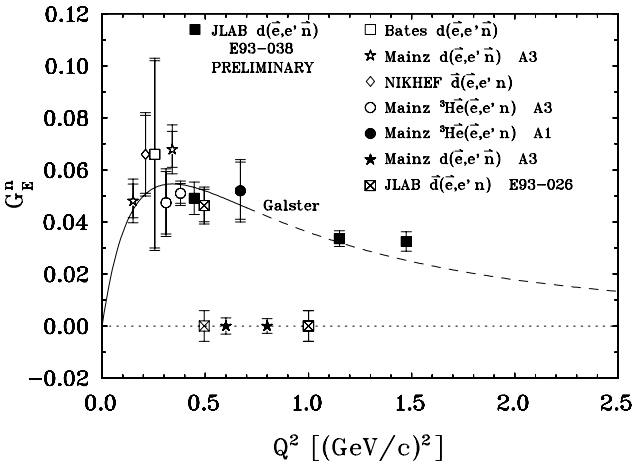

Fig. 4. World data on G_{En} *vs.* Q^2 obtained from polarization measurements. The points on the abscissa ($G_{En} = 0$) are projections.

In the cross ratio method of analysis of the scattering asymmetries measured in the polarimeter, false asymmetries cancel to all orders from helicity-dependent errors in charge integration or system dead-times, or from errors in detection efficiency and acceptances; and the false asymmetries cancel to first order from misalignments with respect to $\vec{q}$, or from a difference in the beam polarization for the two helicity states [4].

Plotted in fig. 3 as a function of the precession angle are the scattering asymmetries for the data at $Q^2 = 1.15$ $(\mathrm{GeV}/c)^2$. Fits to the data are shown for both $p(n,n)p$ elastic scattering events and $p(n,p)n$ charge-exchange events in the front array of the polarimeter. From the dependence $\xi \propto \sin(\chi + \delta)$, we extracted the phase shift δ, and obtained the ratio g from eq. (4).

4 Preliminary results

The extraction of G_{En} from the measured quantity $g \equiv G_{En}/G_{Mn}$ is based on the dipole form factor for G_{Mn} with

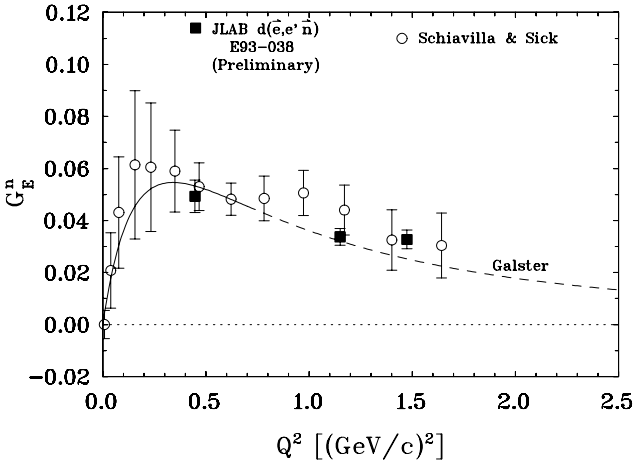

Fig. 5. Comparison of E93-038 data with results extracted from the deuteron quadrupole form factor.

an assumed relative uncertainty of 5%. Preliminary results for G_{En} *vs.* Q^2 are plotted as filled squares in fig. 4. World data on G_{En} from polarization measurements [5–13] are shown too. Data from E93-038 reveal that G_{En} continues to follow the parameterization of Galster *et al.* [14] up to $Q^2 = 1.15$ (GeV/c)^2 and rises above the Galster parameterization at $Q^2 = 1.47$ (GeV/c)^2. There is no theoretical reason for G_{En} to follow the Galster parameterization, which was based on the best fit to the experimental data available on electron-deuteron scattering up to $Q^2 \sim 0.7$ (GeV/c)^2. In fig. 4, the Galster parameterization is plotted as a solid line up to $Q^2 = 0.7$ (GeV/c)^2 and a dashed line thereafter.

Recently, Schiavilla and Sick [15] extracted values of G_{En} from the analysis of t_{20} and T_{20} data on the deuteron, which were measured up to $Q^2 = 1.65$ (GeV/c)^2. The results are shown as circles in fig. 5. The error bars include the spread of theoretical predictions and experimental uncertainties in the deuteron quadrupole form factor. The preliminary results from the E93-038 measurements are plotted as squares also in fig. 5 with error bars that are significantly smaller than those extracted by Schiavilla and Sick from the deuteron quadrupole form factor. The two results are consistent with each other.

Our data will serve to test predictions of various models [16–23]. In fig. 6, we focus on those models [16,20–23] that are closest to the data. Figure 7 shows models (*e.g.*, [17–19,16] without applying constituent-quark form factors) that deviate from the data. A successful model must be able to predict the electric and magnetic form factors of both the neutron and the proton.

5 Systematic uncertainties

A significant advantage of our experimental technique is that the scale and systematic uncertainties are small; in particular, the analyzing power of the polarimeter cancels in the ratio and the beam polarization, P_L, also cancels as it varied little during sequential measurements of the scattering asymmetries. We measured the beam polarization with a Möller polarimeter and changes in P_L were typically on the order of one to two percent. The helicity of the beam was reversed at a frequency of 30 Hz to eliminate instrumental asymmetries. Our systematic uncertainties are listed in table 2. Beam charge asymmetries (of typically 0.1 percent) cancel in the cross ratio. Detector threshold differences cancel also in the cross ratio.

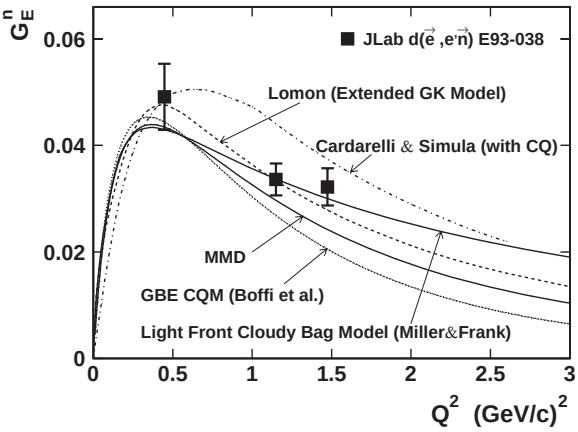

Fig. 6. Selected model predictions for G_{En}.

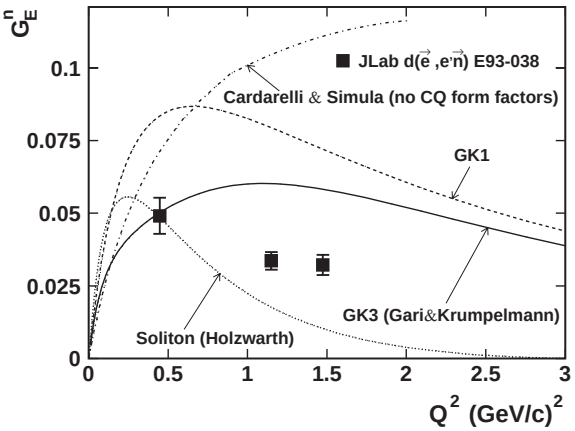

Fig. 7. Models that deviate from the data.

Table 2. The estimated values of the systematic uncertainties in $\Delta g/g$ (%) for each of our Q^2 points.

	Q^2 ((GeV/c)^2)				
Source	$0.45^{(a)}$	$1.17^{(a)}$	$1.14^{(b)}$	$1.47^{(a)}$	$1.47^{(b)}$
Beam polarization	1.4	0.8	0.4	1.7	0.3
Positioning/traceback	0.2	0.3	0.3	0.4	0.4
Precession angle	1.1	0.3	0.1	0.5	0.1
Total	1.8	0.9	0.5	1.8	0.5

$^{(a)}$ $\chi = \pm 40^\circ$ precession.
$^{(b)}$ $\chi = 0^\circ, \pm 90^\circ$ precession.

The false asymmetry or dilution of the asymmetry from the two-step process $^2\mathrm{H}(\vec{e}, e'\vec{p})^1\mathrm{H} + \mathrm{Pb}(\vec{p}, \vec{n})$ was assessed by running with a liquid-hydrogen target. The correction to G_{En} is negligible for $Q^2 = 0.45$ and 1.15 $(\mathrm{GeV}/c)^2$ and small for $Q^2 = 1.47$ $(\mathrm{GeV}/c)^2$.

Afanasev *et al.* [24] calculated the effect of radiative corrections on the ratio of the transverse to longitudinal polarization components. Radiative corrections increase the magnitude of each polarization component by an amount that varies from ∼1.4% to ∼4.7%; however, these effects effectively cancel in the ratio of the scattering asymmetries. The effect of radiative corrections on g is small for $Q^2 = 0.45$ $(\mathrm{GeV}/c)^2$ and negligible for the other values of Q^2.

We have not made a correction at $Q^2 = 0.45$ $(\mathrm{GeV}/c)^2$ for the two-step process $^2\mathrm{H}(\vec{e}, e'\vec{p})^1\mathrm{H} + ^2\mathrm{H}(\vec{p}, \vec{n})$ in the deuterium nucleus; however, this correction was determined to be $65 \pm 3\%$ at $Q^2 = 0.15$ $(\mathrm{GeV}/c)^2$ and $8 \pm 3\%$ at $Q^2 = 0.34$ $(\mathrm{GeV}/c)^2$ [10]. This effect decreases with increasing Q^2 because the (p, n) charge-exchange cross-section decreases with increasing Q^2.

To extract the corrections to g resulting from the finite acceptance of the polarimeter and final-state interactions, we developed the simulation program called GENGEN [25]. GENGEN includes a realistic model of the polarimeter and the electron spectrometer, and the event generator samples events according to the model of Arenhövel *et al.* [26]. The simulated data can be analyzed with the same programs we developed for the analysis of the experimental data. The simulation reproduces experimental distributions of W, Q^2, θ_{nq}, and ϕ_{nq}. Under development is a more refined simulation that will model nuclear interactions and depolarization processes in the lead curtain and will simulate spin precession in the non-uniform dipole field. In progress also are acceptance-averaging calculations based on experimental data; in these calculations, for real neutron tracks reconstructed in NPOL we compute the neutron polarization vector according to the model of Arenhövel *et al.* [26], and precess it through the magnetic-field map of the Charybdis dipole magnet. These corrections need to be applied to the preliminary values of G_{En} reported here.

6 Summary

The new data from JLab E93-038 a) demonstrate the utility of the recoil polarization technique to higher Q^2 than previous experiments; b) sharpen our understanding of the charge density distribution within the neutron and reduce the uncertainty in our knowledge of the interior charge density of the neutron [27]; c) exclude some models; d) reveal that G_{En} continues to follow the Galster parameterization up to $Q^2 = 1.15$ $(\mathrm{GeV}/c)^2$ and rises above the Galster parameterization at $Q^2 = 1.47$ $(\mathrm{GeV}/c)^2$. The results shown here are preliminary. Although only statistical error bars are shown, systematic errors are small compared to statistical errors.

The support of the Jefferson Lab scientific and engineering staff in Hall C and the accelerator staff is gratefully acknowledged. This work was supported in part by the National Science Foundation, the Department of Energy, and the Deutsche Forschungsgemeinschaft. The Southeastern Universities Research Association (SURA) operates the Thomas Jefferson National Accelerator Facility under the U.S. Department of Energy contract DE-AC05-84ER40150.

References

1. R. Madey, T. Eden, Fizika B **8**, 35 (1999).
2. R. Madey, A. Lai, T. Eden, *Polarization Phenomena in Nuclear Physics*, edited by E.J. Stephenson, S.E. Vigelor, AIP Conf. Proc., **339**, 47 (1995).
3. R.G. Arnold, C.E. Carlson, F. Gross, Phys. Rev. C **23**, 363 (1981).
4. G.G. Ohlsen, P.W. Keaton jr., Nucl. Instrum. Methods **109**, 41 (1973).
5. T. Eden *et al.*, Phys. Rev C **50**, R1749 (1994).
6. M. Meyerhoff *et al.*, Phys. Lett. B **327**, 201 (1994).
7. J. Becker *et al.*, Eur. Phys. J. A **6**, 329 (1999).
8. J. Golak *et al.*, Phys. Rev. C **63**, 034006 (2001).
9. M. Ostrick *et al.*, Phys. Rev. Lett. **83**, 276 (1999).
10. C. Herberg *et al.*, Eur. Phys. J. A **5**, 131 (1999).
11. I. Passchier *et al.*, Phys. Rev. Lett. **82**, 4988 (1999).
12. D. Rohe *et al.*, Phys. Rev. Lett. **83**, 4257 (1999).
13. H. Zhu *et al.*, Phys. Rev. Lett. **87**, 081801 (2001).
14. S. Galster, H. Klein, K.H. Schmidt, D. Wegener, J. Blechwenn, Nucl. Phys. B **32**, 221 (1971).
15. R. Schiavilla, I. Sick, Phys. Rev. C **64**, 041002(R) (2001).
16. F. Cardarelli, A. Simula, Phys. Rev. C **62**, 065201 (2000); E. Pace, G. Salme, F. Cardarelli, S. Simula, Nucl. Phys. A **666** & **667**, 33c (2000).
17. M.F. Gari, W. Krumpelmann, Z. Phys. A **322**, 689 (1985).
18. M.F. Gari, W. Krumpelmann, Phys. Lett. B **274**, 159 (1992).
19. G. Holzwarth, Z. Phys. A **356**, 339 (1996).
20. S. Boffi, L.Ya. Glozman, W. Klink, W. Plessas, M. Radici, R.F. Wagenbrunn, Eur. Phys. J. A **14**, 17 (2002); W. Plessas, S. Boffi, L.Ya. Glozman, W. Klink, M. Radici, R.F. Wagenbrunn, Nucl. Phys. A **699**, 312c (2002); R.F. Wagenbrunn, S. Boffi, W. Klink, W. Plessas, M. Radici, Phys. Lett. B **511**, 33 (2001).
21. P. Mergell, U.G. Meissner, D. Drechsel, Nucl. Phys. A **596**, 367 (1996); H.W. Hammer, U.G. Meissner, D. Drechsel, Phys. Lett. B **385**, 343 (1996).
22. E. Lomon, Phys. Rev. C **64**, 035204 (2001), and nucl-th 0203081 (2002).
23. G.A. Miller, M.R. Frank, nucl-th 0201021 (2002); M.R. Frank, B.K. Jennings, G.A. Miller, Phys. Rev. C **54**, 920 (1996).
24. A. Afanasev, I. Akushevich, N. Merenkov, Phys. Rev. D **64**, 113009 (2001).
25. J.J. Kelly, GENGEN computer code, private communication.
26. H. Arenhövel, W. Leidemann, E.L. Tomusiak, Z. Phys. A **331**, 123 (1988).
27. J.J. Kelly, Phys. Rev. C **66**, 065203 (2002), hep-ph/0204239.